ARTICLE

New Insight into Competition between Decomposition Pathways of Hydroperoxymethyl Formate in Low Temperature DME Oxidation

Li-li Xing, Xiao-yuan Zhang, Zhan-dong Wang, Shuang Li, Li-dong Zhang*

National Synchrotron Radiation Laboratory, University of Science and Technology of China, Hefei 230029, China

(Dated: Received on March 30, 2015; Accepted on May 7, 2015)

Hydroperoxymethyl formate is a crucial intermediate formed during the low-temperature oxidation of dimethyl ether. The decomposition pathways of $HOOCH_2OCHO$ were calculated at QCISD(T)/CBS//B3LYP/6-311++G(d,p) level. The temperature- and pressure-dependent rate constants are computed using microcanonical variational transition state theory coupled with the RRKM/master equation calculations. The calculations show that a pathway leads to the formation of formic acid and a Criegee intermediate does exist, besides the direct dissociation channel to OH and OCH_2OCHO radicals. However, formation of the Criegee intermediate has never been considered as an intermediate in dimethyl ether combustion before. The computed rate constants indicate that the newly confirmed pathway is competitive to the direct dissociation route and it is promising to reduce the low-temperature oxidation reactivity. Also electronic effect of groups, *e.g.* -CHO and O atom, is taken into account. Moreover, Hirshfeld atomic charge and natural bond order analysis are performed to explain this phenomenon from a perspective of chemical nature.

Key words: Hydroperoxymethyl formate, RRKM/master equation calculations, Low temperature oxidation, Dimethyl ether, Chain branching

I. INTRODUCTION

Dimethyl ether (DME) appears to be an excellent and efficient alternative fuel for use in diesel engines [1, 2] due to its merits of high cetane number and low soot and NO_x emission tendencies in combustion field. On the other hand, the leakage of DME in transportation and storage may cause an accidental fire because of its high oxidation reactivity even under low temperature. In view of both the advantages and disadvantages in the applications of DME as an alternative, a better understanding of its low-temperature oxidation characteristics is highly desired for the engine design. Extensive experiments [3−11] and theoretical calculations [6, 12−20], as well as kinetic modeling studies [7−9, 21−23], have been carried out for the combustion chemistry of DME in last decades. Curran *et al.* proposed the DME consumption pathways, starting from the parent DME and proceeding along with $CH_3OCH_2\cdot+O_2\rightarrow CH_3OCH_2OO\cdot\rightarrow\cdot CH_2OCH_2O_2H+O_2\rightarrow\cdot OOCH_2OCH_2O_2H\rightarrow OH+HOOCH_2OCHO$ (HPMF) [9]. This reaction sequence for DME consumption has received common consensuses at present. The following decomposition of hydroperoxymethyl formate (*i.e.*, HPMF) then produces the second OH radical through the following reaction R1:

$$HPMF=OCH_2OCHO+OH \qquad R1$$

reaction R1 is one of the most important reactions in low-temperature oxidation of DME. A clear proof can be found in Burke's work about the sensitivity analysis of DME ignition delay time conducted at 10 atm and various equivalence ratios [7]. As we can see, the most-promoting reaction at ϕ=0.5, 1.0, and 2.0 in 'air' is reaction R1, where HPMF acts as a trigger and its decomposition leads to the chain branching step and consequently the occurrence of the first-stage ignition. Recently, Tomlin *et al.* [24] exhibited a global uncertainty analysis for three current mechanisms about DME low-temperature oxidation: Metcalfe *et al.* [21], Zheng *et al.* [25], and Liu *et al.* [26]. Their work highlighted that reaction (R1) and its competitive reactions are likely to dominate the remaining uncertainties in current DME models.

However, despite the importance of HPMF decomposition channels, only a few reports could be found available up to date [12, 16]. Andersen and Carter studied the thermal decomposition of HPMF at the level of B3LYP, they proposed an important branching reaction of reactions R2a and R2b as below, which is theoretically predicted to be more important than reaction R1 at 600 K [12, 16]. In particular, the Criegee biradical ($\cdot CH_2OO\cdot$ in reaction R2b) has also been shown to be an important intermediate in combustion chemistry by

*Author to whom correspondence should be addressed. E-mail: zld@ustc.edu.cn

Taatjes and co-workers, whose recent studies on reactions of $\cdot CH_2OO\cdot$ with aldehydes and ketones demonstrate that these Criegee intermediates could serve as a potential source of acids at low temperatures and pressures [27, 28].

$$HPMF{=}HCOOHCH_2OO \quad \text{R2a}$$

$$HCOOH\cdots CH_2OO{=}CH_2OO{+}HCOOH \quad \text{R2b}$$

Beyond Andersen *et al.*'s calculations [12, 16], little is known about the reaction of HPMF decomposition. A similar species γ-ketohydroperoxide (KHP) in the low-temperature propane oxidation was studied by Jalan *et al.* [29]. The inclusion of Korcek decomposition mechanism of KHP, where a cyclic intermediate is first formed, yielded an excellent agreement with experiment [29]. The great analogy of HPMF with KHP intrigues us to explore the fate of HPMF in low-temperature DME oxidation process. The reaction network of HPMF, especially the competition of other reaction channels with reaction R1, is in a severe lack of knowledge except Andersen *et al.*'s work mentioned above [12, 16]. Therefore, in order to better understand the low-temperature oxidation mechanism of DME, the unimolecular decomposition of HPMF urgently needs detailed calculations with high precision.

In this work, we pursued a high-level computational investigation on the unimolecular decomposition of HPMF. The phenomenological rate constants were computed using the microcanonical variational transition state theory (μVT) coupled with the RRKM/master equation calculations. Moreover, the Hirshfeld atomic charge analysis and natural bond order analysis were performed to compare the different electronic effect between O and CH_2 group on KHP and HPMF unimolecular decomposition in detail. These reactions represent a new general class of reactions and are expected to play an important role in the low-temperature DME oxidation mechanism. We hope that these results can shed helpful insight into understanding the low-temperature oxidation reactivity of DME and lead to further development of a comprehensive DME low-temperature oxidation mechanism in the future.

II. THEORETICAL METHODS

A. Quantum chemical methods

The stationary points involved in unimolecular decomposition pathways of HPMF were geometrically optimized at the B3LYP/6-311++G(d,p) level. Based on optimized structures, two separate methods were used to perform the single-point energy calculations: quadratic configuration interaction with singles, doubles and perturbative inclusion of triples (QCISD(T)) [30, 31], and Møller-Plesset perturbation theory (MP2). The QCISD(T) calculations were done with two Dunning basis sets [30, 32]: the correlation-consistent, polarized-valence, double-ζ (cc-PVDZ) and triple-ζ (cc-pVTZ). The MP2 calculations were done with three Dunning basis sets: cc-pVDZ, cc-pVTZ and cc-pVQZ (quadruple-ζ). The means of obtaining energy at complete basis set limit (CBS) were referred to those used by Goldsmith *et al.* [33], being expressed as:

$$E_{(\mathrm{QCISD(T)/CBS})} = E_{(\mathrm{QCISD(T)/CBS})_{\mathrm{DZ}\to\mathrm{TZ}}} + E_{(\mathrm{MP2/CBS})_{\mathrm{TZ}\to\mathrm{QZ}}} - E_{(\mathrm{MP2/CBS})_{\mathrm{DZ}\to\mathrm{TZ}}} \quad (1)$$

Each term on the right-hand side represents an individual CBS approximation extrapolated by energies at designated basis sets. For instance, $E_{(\mathrm{QCISD(T)/CBS})_{\mathrm{DZ}\to\mathrm{TZ}}}$ represents the CBS energy extrapolated by QCISD(T)/cc-pVDZ and QCISD(T)/cc-pVTZ energies, as the following expression:

$$E_{(\mathrm{QCISD(T)/CBS})_{\mathrm{DZ}\to\mathrm{TZ}}} = E_{(\mathrm{QCISD(T)/cc\text{-}pVTZ})} + 0.4629[E_{(\mathrm{QCISD(T)/cc\text{-}pVTZ})} - E_{(\mathrm{QCISD(T)/cc\text{-}pVDZ})}] \quad (2)$$

Similar formula also applies to the other two terms as following:

$$E_{(\mathrm{MP2/CBS})_{\mathrm{TZ}\to\mathrm{QZ}}} = E_{(\mathrm{MP2/cc\text{-}pVQZ})} + 0.6938[E_{(\mathrm{MP2/cc\text{-}pVQZ})} - E_{(\mathrm{MP2/cc\text{-}pVTZ})}] \quad (3)$$

$$E_{(\mathrm{MP2/CBS})_{\mathrm{DZ}\to\mathrm{TZ}}} = E_{(\mathrm{MP2/cc\text{-}pVTZ})} + 0.4629[E_{(\mathrm{MP2/cc\text{-}pVTZ})} - E_{(\mathrm{MP2/cc\text{-}pVDZ})}] \quad (4)$$

The approximation method has been proven to be efficient and accurate for high-level energy estimations with the uncertainty within 0.9 kcal/mol [33]. The zero-point energy corrections were obtained from the B3LYP/6-311++G(d,p) optimizations.

With respect to the barrierless reaction R1, there is no chemical barrier along the reaction coordinate. To properly treat this reaction, the minimum energy path describing the bond fission process was constructed with a step size of 0.2 Å using the CASPT2(2e,2o)/cc-pVTZ method. Here the minimum active space (2e,2o) was used, which simply contains the σ and σ^* orbitals for the breaking bond. Then the energies for each point along the dissociation pathway were scaled by the bond dissociation energy computed at QCISD(T)/CBS level. The Hirshfeld atomic charge analysis [34] of some important species was carried out at B3LYP/6-311++G(d,p) using the electronic density of the molecule and of a fictitious promolecule, which has been suggested to yield chemically meaningful charges and show little basis set dependence [35, 36]. Traditionally, all main reaction channels were investigated with the natural bond order analysis to reveal the reaction mechanism. All the single-reference calculations were performed with the Gaussian 09 program [37] and the multi-reference calculations were done with the Molpro program [38].

DOI:10.1063/1674-0068/28/cjcp1503053

B. Rate constant calculations

The μVT was applied for the C−O and O−O bond dissociation channels. In the μVT principle, the high pressure limit (HPL) rate constant was calculated as a function of energy and position of the transition state, *i.e.*, $k_{\mathrm{HPL}}(E)$ was calculated at each point along the reaction coordinate. At each energy, the optimum transition state is located at the position with the minimum $k_{\mathrm{HPL}}(E)$. After that, the microcanonical rate constants of all channels, with or without chemical barriers, were computed by the RRKM theory, which was coupled with master equation simulations to export the phenomenological rate constants at various temperature and pressure. The Eckart tunneling correction [39] was included in the RRKM/master equation calculations for reactions with tight transition state (TS). As for the collisional model used in the master equation simulations, the interaction between reactants and the bath gas Ar was modeled by the Lennard-Jones (L-J) potential. The L-J parameters were chosen as σ=3.465 Å, ε=113.5 K for Ar [40]. For HPMF, the L-J parameters were estimated according to the empirical equations [41]:

$$\sigma = 2.44\left(\frac{T_{\mathrm{c}}}{P_{\mathrm{c}}}\right)^{1/3} \tag{5}$$

$$\frac{s_A}{k_{\mathrm{B}}} = 0.77T_{\mathrm{c}} \tag{6}$$

here, k_{B} is the Boltzmann constant, T_{c} is the critical temperature and P_{c} is the critical pressure; the method of Constantinou and Gani [42] was used to estimate the values of T_{c} and P_{c}. According to Eq.(8) and Eq.(9), the L-J values for HPMF were calculated to be σ=5.227 Å and ε=463.5 K, respectively. The collision energy transfer was treated using a single-parameter exponential down model: $\langle\Delta E\rangle_{\mathrm{down}}$=150$(T/300)^{0.85}$ cm^{-1}. Moreover, special consideration was given to low frequency vibrational modes corresponding to internal hindered rotations. These modes were treated as hindered rotors by B3LYP/6-311++G(d,p) hindrance potentials, which were used to compute the partition functions with the hindered rotor approximation. The hindrance potentials were scanned every 30° with all degrees of freedom relaxed but the torsional coordinate. Partition functions were evaluated at the E resolved level and all the kinetic calculations were performed using the master equation code PAPER developed by Georgievskii *et al.* [43].

III. RESULTS AND DISCUSSION

A. Electronic structure calculations

The decomposition of HPMF can occur via many chemically accessible product channels, as listed in Table I. Here seven main channels were identified:

TABLE I Calculated main reaction channels of HPMF decomposition in this work.

Channel 1	HPMF→OCH_2OCHO+OH		R1
Channel 2	HPMF→CH_2OO+HCOOH		R2
	HPMF=INT2	TS2	R3
	INT2→CH_2OO+HCOOH		R4
Channel 3	HPMF=INT2	TS2	R3
	INT2→2HCOOH	TS3	R5
Channel 4	HPMF=INT2	TS2	R3
	INT2→CH_2O+HOC(=O)OH	TS4	R6
Channel 5	HPMF→HCOOH+OH+CHO	TS5	R7
Channel 6	HPMF→CH(=O)OCH(=O)+H_2O	TS6	R8
Channel 7	HPMF→CH(=O)OOH+CH_2O	TS7	R9

channel 1 represents R1, channel 2 represents the CH_2OO and HCOOH formation pathways including R2, R3 and R4, and channels 3, 4, 5, 6, and 7 represent R3+R5, R3+R6, R7, R8, and R9, respectively. The optimized geometries of the saddle points, rotational constants and vibrational frequencies of all species involved in the reactions at the B3LYP/6-311++G(d,p) level are shown in the supplemental materials. Unless a special statement, for the bond dissociation process, the open shell calculations were adopt. The potential energy surface (PES) for HPMF decomposition obtained at QCISD(T)/CBS level is shown in Fig.1. We also displayed the enthalpies of reaction at 298 K for two important product channels using three different methods in Table II. The results at the QCISD(T)/CBS level agree quite well with the data from the NIST Chemistry WebBook [44], implying that the present methodology we used for CBS energy extrapolation is reasonable and reliable.

1. The chain branching step: channel 1

The simple O−O bond fission dissociation of HPMF leading to radical products (OH and OCH_2OCHO) possesses no saddle point along the reaction coordinate, as shown in Fig.2, and the dissociation energy is predicted to be 41.64 kcal/mol. Previous studies reported O−O bond dissociation energies (BDEs) to be 41.6±1 and 42.6±1 kcal/mol for CH_3CH_2OOH [45] and CH_3OOH [46], respectively, and the size effect of the alkyl group on O−O bond strength is assumed to be limited [47]. The BDE of O−O bond for the well-known species γ-ketohydroperoxide (KHP) in low-temperature oxidation of propane was reported to be 49.5 kcal/mol [29], which is much higher than that of HPMF. As we know, 'electron clouds' consisting of electrons are negatively charged, a repulsive potential is normally present between adjacent electron clouds, and this potential tends to push other electron clouds farther away. In general, the repulsion potential from lone pair electrons

DOI:10.1063/1674-0068/28/cjcp1503053

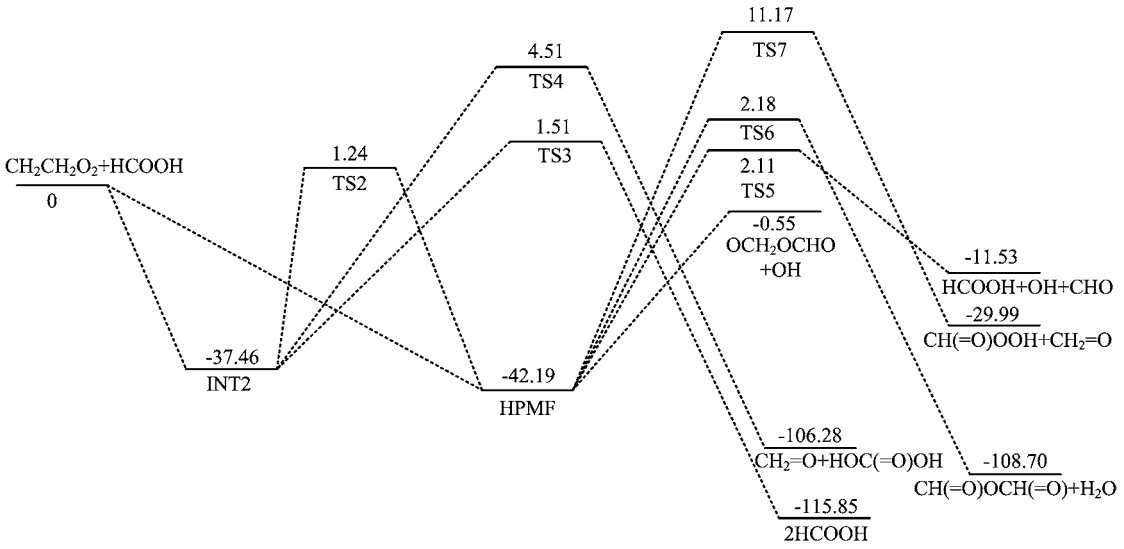

FIG. 1 Potential energy surface of HPMF decomposition at the level of QCISD(T)/CBS//B3LYP/6-311++G(d,p). The energies are in unit of kcal/mol.

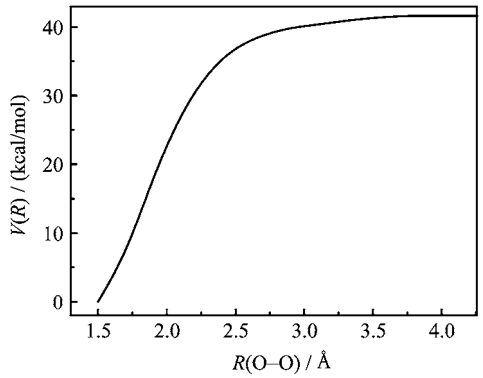

FIG. 2 The dissociation curve at the level of CASPT2(2,2)/cc-pVTZ and scaled by the dissociation energy computed at QCISD(T)/CBS for R1.

TABLE II Enthalpies of major channels in decomposition reaction of HPMF (kcal/mol, 298 K).

	NIST [44]	QCISD(T)/CBS	CBS-QB3	G3B3
R1	43.22	44.19	45.54	41.57
R2	45.31 [16]	45.78	44.84	47.78

is greater than repulsion from bonding pair electrons. Additionally, the negatively-charged lone pairs are typically localized on one single atom, so the dipole moment is prone to be affected by the large, negative, charge population. The difference in BDEs of O−O dissociation between HPMF and KHP can be attributed to the lone pair electron effect on the oxygen atom of the neighboring carbonyl group. In order to explain the difference between KHP and HPMF dissociation channels, additional analysis on the electronic effect, such as charge distribution, could be useful, which will be discussed in more detail later.

2. Formation of CH_2OO and HCOOH

Reaction R2 mainly involves the transfer of H-atom in -OOH group accompanied by simultaneous cleavage of the C6−O7 bond, with no well-defined saddle point in the process. Figure 3 shows the dissociation curve along the stretching bond length in 0.2 Å interval using the CCSD(T)-F12a/cc-pVTZ//M062X/6-311+G(2df,2p) method. This method is adopted by reference to the KHP work of Jalan *et al.* [29] and has been found to provide reliable results. Also the CCSD(T) T1 diagnostics for stationary points indicate that there is no need to perform the multi-reference calculations.

As shown in Fig.4, the atomic label for main species will be used in the following discussion. In addition to R2, there is an alternative reaction mechanism leading to the formation of CH_2OO and HCOOH, namely R3+R4. The H atom in -OOH is transferred to O9 of carbonyl group, during which the O2 atom approaching towards the C8 atom. As reaction proceeds, a five-member-ring intermediate (INT2, R3) arises. A saddle point (TS2) can be readily located at B3LYP/6-311++G(d,p) level for this isomerization reaction. Following that, INT2 directly decomposes into two separate fragments CH_2OO and HCOOH through simultaneous bond fission of C6−O7 and C8−O2. This dissociation process features no well-defined saddle points, and here was preferably treated with the variational transition state theory.

This alternative reaction mechanism is similar to Korcek decomposition of KHP in low-temperature alkane oxidation [29], where a cyclic intermediate is formed via TS_c in Fig.4. The calculated energy barrier

DOI:10.1063/1674-0068/28/cjcp1503053

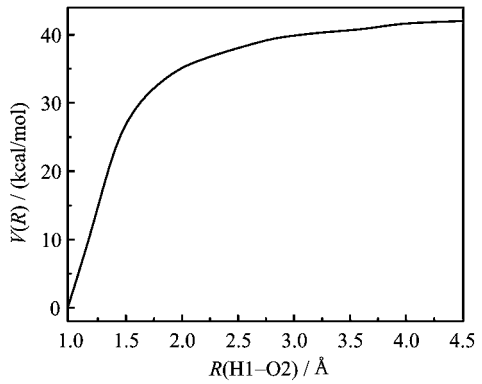

FIG. 3 The dissociation curve at the level of UCCSD(T)-F12a/cc-pVTZ//M062X/6-311+G(2df,2p) and scaled by the dissociation energy computed at QCISD(T)/CBS for R2.

(TS2) for HPMF cyclization is 43.43 kcal/mol, slightly higher than the asymptotic threshold energy of R1 (41.64 kcal/mol). In contrast, the KHP cyclization energy barrier is about 34.7 kcal/mol, which is much lower than threshold energy of the O−O bond fission channel (∼49.5 kcal/mol) [29]. We now attempt to interpret the deviation from two perspectives of molecules: charge distribution and natural bond order. The Hirschfeld atomic charge distribution in TS2 and TS_c is shown in Fig.4. It is amazing that the O2 in TS2 has twice more negative charge than the O2 in TS_c. The conjugated effect is gradually destroyed as the H atom transfers to O9. However, the charge distribution on C8−O2 bond is quite different in these two saddle points. For TS2, the charge assigned to C8 and O2 atoms is far in excess of that required for the formation of nominal C−O bond. The resulting effect is such that this structure is more like a biradical as opposed to TS_c where the charge distribution on C8−O2 bond is close to that required to form nominal C−O bond. It is well known that these biradicals or analogous biradicals could attract the atomic charge of the radical center, leading to stronger charge localization. This localization causes the loss of molecular stabilization and the increase of energy.

The natural bond order analysis for these four molecules is also shown in Fig.4. It is clearly seen that the forming C8−O2 bond has different bond order in TS2 and TS_c. A bond order of 0.3140 in TS2 indicates that it is still far from the formation of a nominal C−O bond, while the bond order of 0.5124 in TS_c is more or less of the same magnitude as that for forming the nominal C−O bond. The comparatively longer bond length of C−O in TS2 gives further proof to the fact that this structure is more like a biradical and has higher energy. Both the charge distribution and bond order analysis help to explain why the cyclization energy barrier of HPMF is higher than KHP, and the energy difference is 8.73 kcal/mol here.

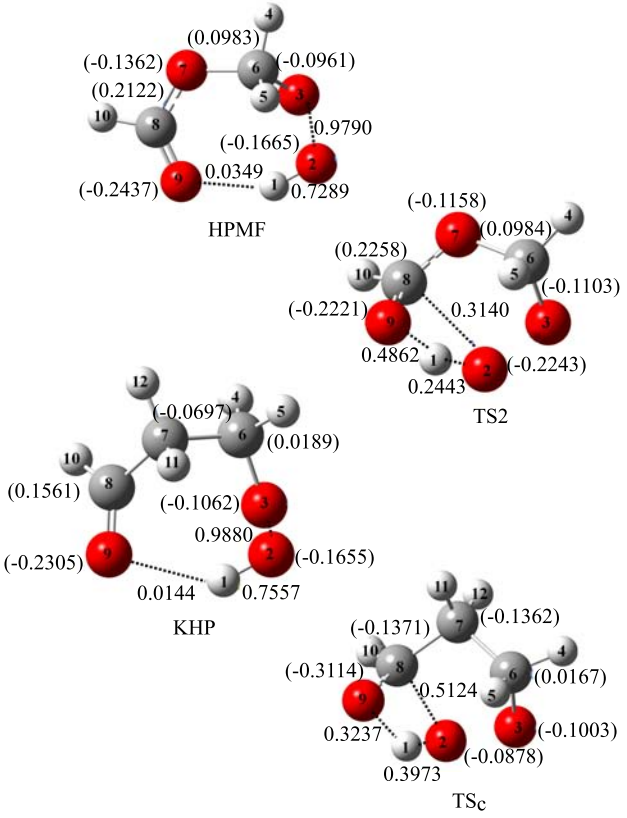

FIG. 4 Hirschfeld atomic charges distribution (values shown in brackets) and natural bond order distribution on the labeled atoms/bonds for HPMF, TS2, KHP and TS_c at the B3LYP/6-311++G(d,p) level.

In order to better understand the electronic effect of O atom after substituting -CH_2 group, more theoretical calculations were performed at the same level of CCSD(T)-F12a/cc-pVTZ//M062X/6-311+G(2df,2p) for adding -CH_2 group to HPMF and KHP. The structures of HPMF, KHP and the reactants after adding CH_2 group are provided in Fig.5. The nomenclature of the species is HPMF-CH_2-a ($HOOCH_2CH_2OCHO$), HPMF-CH_2-b ($HOOCH_2OCH_2CHO$), and KHP-CH_2 ($HOOCH_2CH_2CH_2CHO$), respectively. Figures 6, 7, and 8 show potential energy surfaces of the main decomposition channels for these species, respectively. Comparing the BDEs of O−O bonds in these three molecules, it is obvious to get the conclusion as follows: HPMF-CH_2-a (50 kcal/mol)>HPMF-CH_2-b (47 kcal/mol)>HPMF (41.64 kcal/mol), which can be explained by the electronic effect. The magnitude of inductive effect is also dependent on the distance between the effect and the atom. The inductive effect can be used to determine the stability of a molecule dependent on the charge present on the atom and the groups bonded to it. From our calculations, not only the carbonyl group but also oxygen atom (O7) has an unneglectable inductive influence on the O−O bond dissociation. For cyclization process with well-defined

DOI:10.1063/1674-0068/28/cjcp1503053

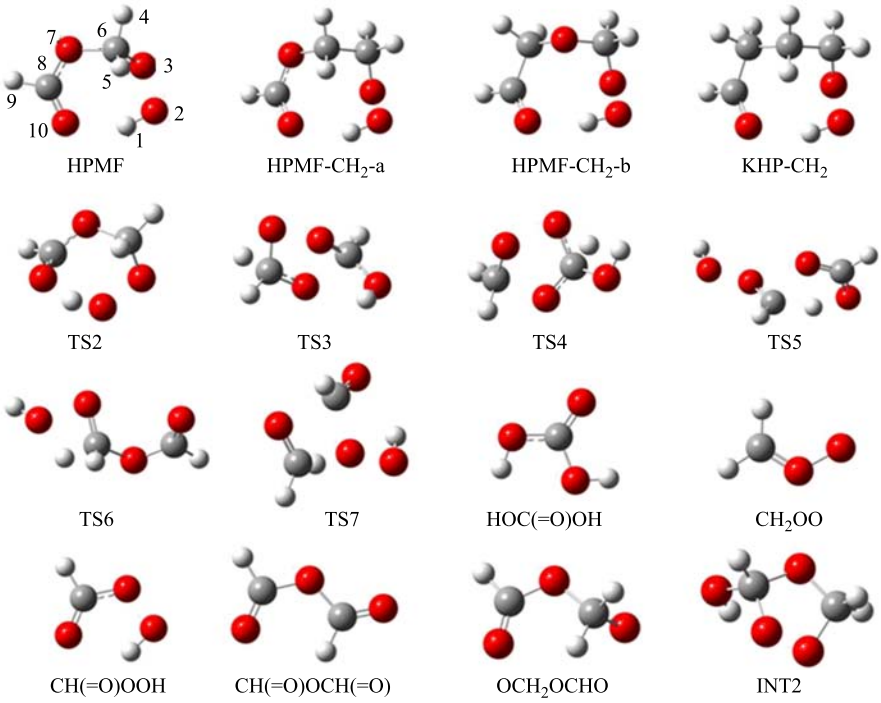

FIG. 5 Optimized geometries of the reactants, transition states, products, and intermediates at the B3LYP/6-311++G(d,p) level. The number on HPMF denotes the atomic label.

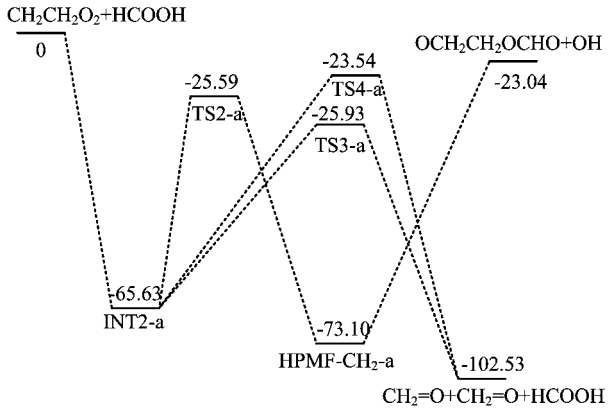

FIG. 6 Potential energy surface of HPMF-CH_2-a decomposition at the level of CCSD(T)-F12a/cc-pVTZ//M062X/6-311+G(2df,2p). The energies are in unit of kcal/mol.

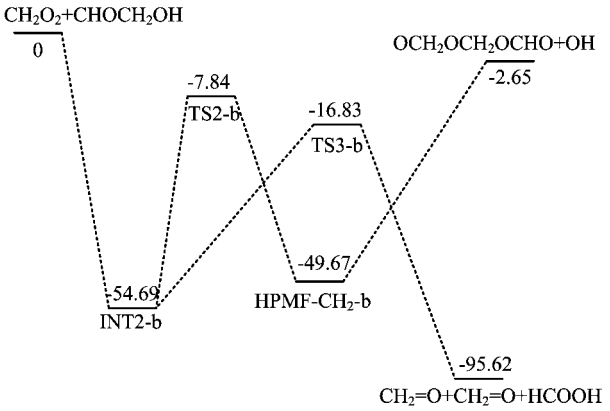

FIG. 7 Potential energy surface of HPMF-CH_2-b decomposition at the level of CCSD(T)-F12a/cc-pVTZ//M062X/6-311+G(2df,2p). The energies are in unit of kcal/mol.

saddle points, the energy barriers have the trend as follows: HPMF-CH_2-a (47.5 kcal/mol)>HPMF (43.4 kcal/mol)>HPMF-CH_2-b (41.86 kcal/mol). With regard to KHP, adding CH_2 to the chain has little effect on the BDE of O−O bond. However it has a great influence on the cyclization process. This is due to the contribution of the additional CH_2 group, which weakens the electronic effect of the C=O for KHP-CH_2, thus leading to a slightly higher energy barrier. Traditionally, as the chain atom number increases, the transition state for H atom transfer and cyclization process is more like a biradical which leads to stronger charge localization and its instability. The additional charge analysis and bond order analysis also provide evidence for these changes in chemical characters, which are provided in the supplemental materials.

As shown in Fig.1, there are other two channels (R5 and R6) from INT2. R5 involves concerted cleavage of the O2−O3 and C8−O7 bonds accompanied by a 1,2 H-shift from C6 to O3 leading to two HCOOH fragments. The overall reaction INT2→2HCOOH has a forward barrier of 38.97 kcal/mol (TS3) and is 78.39 kcal/mol exothermic. For R6, INT2 involves con-

DOI:10.1063/1674-0068/28/cjcp1503053

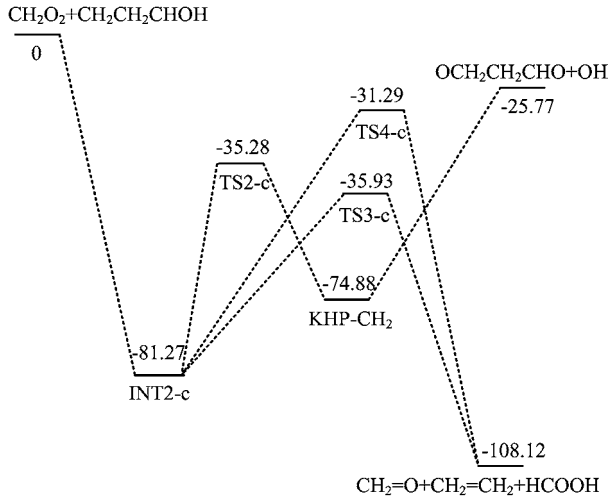

FIG. 8 Potential energy surface of HPMF-CH_2-c decomposition at the level of CCSD(T)-F12a/cc-pVTZ//M062X/6-311+G(2df,2p). The energies are in unit of kcal/mol.

certed cleavage of the O2−O3 and C6−O7 bonds accompanied by a 1,2 H-shift from C8 to O7 leading to $H_2C(=O)$ and HOC(=O)OH fragments. This reaction INT2→$H_2C(=O)$+HOC(=O)OH has a forward barrier of 41.97 kcal/mol (TS4) and is 68.82 kcal/mol exothermic.

3. Other reaction pathways

Beside the aforementioned reactions, there are other reaction pathways for HPMF decomposition. HPMF can directly decompose into three fragments (OH, HCO, HC(=O)OH) via reaction R7 through TS5. The geometry of TS5 features the properties: R(O2−O3)=1.600 Å, R(C6−O7)=2.066 Å, and H atom in -CH_2 group transferring to O9. Figure 1 shows that R7 has an energy barrier of 44.30 kcal/mol. Another decomposition pathway of HPMF is the dehydration reaction R8, by overcoming a barrier of 44.37 kcal/mol (TS6). At last, the most unfavorable pathway is R9, which occurs via a tight four-centered cyclic transition state TS7 with a high energy barrier of 53.36 kcal/mol. These pathways were also included in the RRKM/Master equation calculations.

In summary, the decomposition of HPME can proceed along via barrierless reactions R1 and R2 into different products. It can also occur via reactions with well-defined chemical barriers, among which reaction R3, forming a five-member-ring intermediate (INT2), has the lowest energy barrier TS2. Subsequent dissociation of the intermediate directly gives rise to formic acid and CH_2OO by reaction R4. The reaction sequence HPMF→INT2→HCOOH+CH_2OO provides an alternative mechanism to the formation of formic acid and CH_2OO. The energy of TS2 is of similar magnitude to asymptotic dissociation energies of R1 and R2, despite the fact that R1 and R2 render a significant contribution to overall rates because of entropic effect, we still expect this alternative mechanism to play a certain role in following kinetic predictions. Competition among multiple reactions will be explored in detail later. The present kinetic predictions deviate somewhat from the theoretical calculations by Andersen and Carter [12, 16], which can be owing to the different theoretical methodologies and treatments for the barrierless reaction pathways (R1, R2, and R4).

B. Reaction rate constants

As mentioned above, there are nine possible reaction pathways (R1−R9) for the unimolecular decomposition of HPMF. In this work, we carried out the RRKM/master equation calculations for the major competitive reactions (R1−R9) utilizing the PAPER code developed by Georgievskii *et al.* [43], with the temperature at 400−1300 K and the pressure ranging from 0.01 atm to 10 atm using Ar as the bath gas. Labels $k1$, $k2$, $k3$, $k4$, $k5$, $k6$, and $k7$ represent the global rate constants for the channels 1, 2, 3, 4, 5, 6, and 7 respectively.

Figure 9 shows the calculated rate constants at 0.1 and 10 atm, respectively. For these channels, the rate order is $k2>k1>k6>k5>k3>k4>k7$ at 10 atm in the investigated temperature range. Among them, the rate constants of channel 1 and 2 are obviously larger than those of remaining channels due to the smaller bond dissociation energy and the loose transition state. For the other channels (*i.e.* channels 3−7) with tight transition states, the enthalpies of the transition states have great contribution to the rate constants. Quantum chemical calculations and kinetic predictions both conform to the conclusion that the dominant channels for HPMF dissociation are HPMF→OH+OCH_2OCHO (channel 1) and HPMF→CH_2O_2+HCOOH (channel 2). The predicted global rate constants for individual HPMF decomposition pathway at various temperatures and pressures are displayed in Table III. Moreover, two 3D plots of rate constants for channels 1 and 2 as a function of temperature and pressure are illustrated in Fig.10 and Fig.11, respectively. Due to the significance of channels 1 and 2, the competition between these two channels will be discussed below.

The channel 1 (*i.e.* R1) is a barrierless reaction. The variational principle of transition state theory applied to this reaction requires one to maximize the free energy of activation. The entropic change becomes larger as the separation between the fragments in transition state region increases. As the temperature increases, the entropic effect constitutes a larger contribution to the free energy of activation, and the optimum transition state moves to smaller separation of the fragments in order to maximize free energy of activation. Due to the

DOI:10.1063/1674-0068/28/cjcp1503053

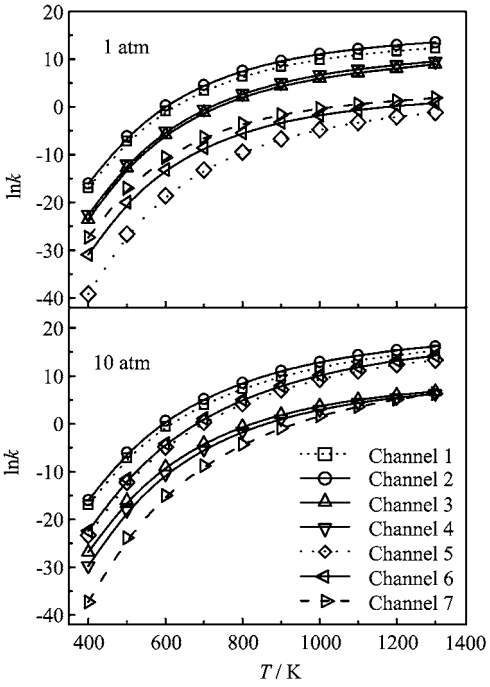

FIG. 9 Calculated rate constants at 400−1300 K, 1 and 10 atm by PAPER of reactions in this work.

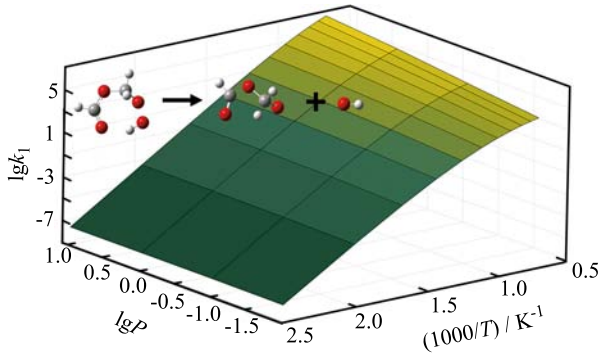

FIG. 10 Calculated rate constants for channel 1 as a function of temperature and pressure.

large entropic effect, it is understood that the reaction R1, forming OH+OCH_2OCHO products, becomes very competitive with the reaction R3 forming an intermediate via a barrier. However, Fig.9 shows that channel 2 forming CH_2OO+HCOOH present a very strong competition with channel 1 (*i.e.*, R1), especially at higher temperatures. This can be easily explained when we note that channel 2 involves contribution from one barrierless dissociation reaction R2, which becomes important similarly because of the entropic effect. As the pressure increases, channel 2 becomes more and more competitive with channel 1. The new competition between OH+OCH_2OCHO and CH_2OO+HCOOH channels is different from the previous work [16] owing to the different treatment for the barrierless dissociation channels. In this work, the barrierless reaction R2 leading to the CH_2OO and HCOOH formation is treated with the μVT theory as mentioned before.

TABLE III Calculated global rate coefficients of HPMF dissociation channels in this work.

Reaction	A	n	E	P/atm
Channel 1	5.77×10^{20}	−2.15	41289	HPL
	8.66×10^{58}	−14.66	51663	0.01
	2.88×10^{54}	−12.98	51439	0.10
	1.79×10^{45}	−9.91	49186	1.00
	2.54×10^{36}	−7.04	46743	10.0
Channel 2	1.57×10^{34}	−6.15	46128	HPL
	1.73×10^{61}	−15.19	52637	0.01
	5.95×10^{55}	−13.21	51978	0.10
	1.70×10^{48}	−10.64	50416	1.00
	1.52×10^{43}	−8.96	49222	10.0
Channel 3	4.51×10^{15}	−1.24	44070	HPL
	4.76×10^{65}	−18.30	55738	0.01
	4.96×10^{64}	−17.46	56973	0.10
	2.85×10^{59}	−15.38	57022	1.00
	1.46×10^{50}	−12.17	55289	10.0
Channel 4	4.49×10^{20}	−2.62	48936	HPL
	1.86×10^{55}	−15.14	55726	0.01
	6.37×10^{59}	−15.96	58058	0.10
	5.38×10^{59}	−15.41	59806	1.00
	3.14×10^{53}	−13.10	59280	10.0
Channel 5	2.30×10^{13}	0.21	44007	HPL
	3.99×10^{58}	−15.02	54806	0.01
	1.09×10^{56}	−13.75	55792	0.10
	4.15×10^{46}	−10.45	54245	1.00
	3.29×10^{35}	−6.75	51535	10.0
Channel 6	1.10×10^{11}	1.03	42969	HPL
	2.71×10^{56}	−14.29	53502	0.01
	1.45×10^{54}	−13.10	54791	0.10
	5.67×10^{44}	−9.79	53277	1.00
	2.10×10^{34}	−6.29	50850	10.0
Channel 7	3.33×10^{15}	−0.78	54293	HPL
	9.58×10^{48}	−13.32	60721	0.01
	1.24×10^{55}	−14.44	63220	0.10
	2.43×10^{52}	−12.89	64444	1.00
	1.48×10^{44}	−9.87	63624	10.0

Note: HPL are high pressure limit, units: s^{-1} and cal/mol. Rate coefficient=$AT^n\exp(-E/RT)$, where T is in K and E is in cal/mol, while A has unit of s^{-1}.

The branching ratios shown in Fig.12 also demonstrate the competition among main channels in this system. Figure 12 also plots the results from previous work by Andersen *et al.* [12, 16] for comparison (channels 1^* and 2^*). The branching ratio of channel 1 has little temperature dependence, whereas branching of channel 1^* by Andersen *et al.* shows a strong posi-

DOI:10.1063/1674-0068/28/cjcp1503053

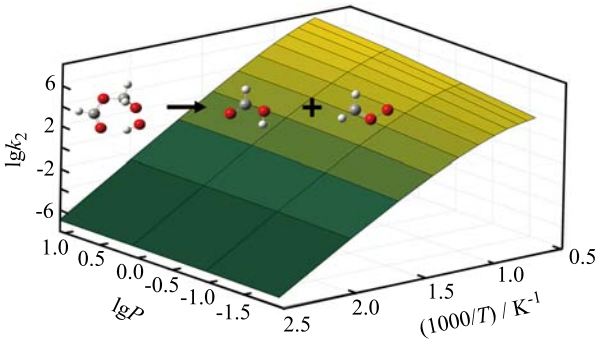

FIG. 11 Calculated rate constants for channel 2 as a function of temperature and pressure.

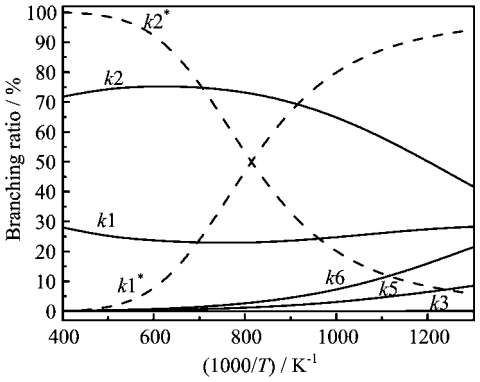

FIG. 12 Branching ratios for five main reaction channels at high pressure limit and 400−1300 K. Here $k1$, $k2$, $k3$, $k5$, and $k6$ represent channel 1, 2, 3, 5, and 6 respectively, * denotes the result from Andersen *et al.* [16].

tive temperature dependence. The branching curves for channels 1 and 1* intersect at ∼700 K. For channel 2, current branching results show that it always plays an important role in the investigated temperature range, while Andersen *et al.* reported a decreasing branching ratio with increasing temperature for this channel. The large discrepancy in branching ratios simply stems from the disparate rate constants by Andersen *et al.* and present study. Andersen *et al.* predicted the rate constants of CH_2OO+HCOOH product channel to be ten times larger than those of OH+OCH_2OCHO channel at 600 K, whereas at the same temperature, the present study predicts the CH_2OO+HCOOH channel to be three times faster.

As a conclusion, the branching ratios between these two channels, OH+OCH_2OCHO and CH_2OO+HCOOH, were found to present some new insights. The new competition between these two channels will have different effect on the low-temperature oxidation reactivity of DME compared to Andersen's work.

IV. CONCLUSION

In this work, the reaction pathways of HPMF decomposition were investigated in detail by high-level quantum chemistry calculations. The microcanonical variational transition state theory calculations coupled with the RRKM/master equation calculations were performed, which provide evidence and theoretical rate coefficients for new competing relationship about HPMF unimolecular dissociation in low-temperature oxidation of DME. The H atom transfer and simultaneous cyclization reaction has high barrier height despite the low angle strain of the five-membered ring intermediate, which can be explained by extra electronic effects revealed by the change of charge distribution in the reaction processes. It is worth mentioning that the rate constants of reactions affecting the oxidation reactivity of DME at relatively low temperatures should be reviewed considering the new competing relationship, *i.e.* the CH_2OO and HCOOH formation channel plays an unignored role compared with the OH direct dissociation. Thus the new competing relationship will greatly decrease the low-temperature oxidation reactivity of DME.

Supplementary materials: Geometries, vibrational frequencies, and rotational constants of HPMF, INT2, OCH_2OCHO, CH_2OO, CH(=O)OCH(=O), CH(=O)OOH, HOCOOH, TS2, TS3, TS4, TS5, TS6, TS7, HPMF-CH_2-a, HPMF-CH2-b, KHP-CH_2, INT2-a, TS2-a, TS3-a, TS4-a, INT2-b, TS2-b, TS3-b, INT2-c, TS2-c, TS3-c, TS4-c, OCH_2CH_2OCHO, CH_2CH_2OO, OCH_2OCH_2CHO, CH_2CH_2CHOH, $CHOCH_2OH$, and $OCH_2CH_2CH_2CHO$ at the level of B3LYP/6-311++G(d,p) are given.

V. ACKNOWLEDGMENTS

This work was supported by the National Key Scientific Instruments and Equipment Development Program of China (No.2012YQ22011305), the National Natural Science Foundation of China (No.21373193 and No.U1232127), and the Chinese Universities Scientific Fund (No.WK2320000020). We highly appreciate Dr. Georgievskii Yuri and Dr. Stephen J. Klippenstein from Chemical Sciences and Engineering Division (Argonne National Laboratory, USA) for their help on using the PAPER program. We also appreciate Dr. Fei Qi, Dr. Feng Zhang, Dr. Yu-yang Li and Li-li Ye from University of Science and Technology of China for their useful discussions.

[1] C. Arcoumanis, C. Bae, R. Crookes, and E. Kinoshita, Fuel **87**, 1014 (2008).
[2] K. Kohse-Höinghaus, P. Oßwald, T. A. Cool, T. Kasper, N. Hansen, F. Qi, C. K. Westbrook, and P. R. Westmoreland, Angew. Chem. Int. Edit. **49**, 3572 (2010).
[3] F. Herrmann, P. Oßwald, and K. Kohse-Höinghaus, Proc. Combust. Inst. **34**, 771 (2013).

DOI:10.1063/1674-0068/28/cjcp1503053

[4] H. Guo, W. Sun, F. M. Haas, T. Farouk, F. L. Dryer, and Y. Ju, Proc. Combust. Inst. **34**, 573 (2013).
[5] K. Suzaki, K. Tsuchiya, M. Koshi, and A. Tezaki, J. Phys. Chem. A **111**, 3776 (2007).
[6] T. Yamada, J. W. Bozzelli, and T. H. Lay, Int. J. Chem. Kinet. **32**, 435 (2000).
[7] U. Burke, K. P. Somers, P. O'Toole, C. M. Zinner, N. Marquet, G. Bourque, E. L. Petersen, W. K. Metcalfe, Z. Serinyel, and H. J. Curran, Combust. Flame doi:10.1016/j.combustflame.2014.08.014 (2014).
[8] Z. Wang, X. Zhang, L. Xing, L. Zhang, F. Herrmann, K. Moshammer, F. Qi, and K. Kohse-Höinghaus, Combust. Flame doi:10.1016/j.combustflame.2014.10.003 (2014).
[9] H. J. Curran, S. L. Fischer, and F. L. Dryer, Int. J. Chem. Kinet. **32**, 741 (2000).
[10] N. Kurimoto, B. Brumfield, X. Yang, T. Wada, P. Diévart, G. Wysocki, and Y. Ju, Proc. Combust. Inst. doi:10.1016/j.proci.2014.05.120 (2014).
[11] P. Dagaut, C. Daly, J. M. Simmie and M. Cathonnet, *The Oxidation, and Ignition of Dimethylether from Low to High Temperature (500-1600 K): Experiments and Kinetic Modeling*, Pittsburgh: Combustion Institute, (1998).
[12] A. Andersen and E. A. Carter, J. Phys. Chem. A **107**, 9463 (2003).
[13] Q. S. Li, Y. Zhang, and S. Zhang, J. Phys. Chem. A **108**, 2014 (2004).
[14] C. M. Rosado-Reyes, J. S. Francisco, J. J. Szente, M. M. Maricq, and L. Frøsig Østergaard, J. Phys. Chem. A **109**, 10940 (2005).
[15] K. Suzaki, N. Kanno, K. Tonokura, M. Koshi, K. Tsuchiya, and A. Tezaki, Chem. Phys. Lett. **425**, 179 (2006).
[16] A. Andersen and E. A. Carter, Mol. Phys. **106**, 367 (2008).
[17] R. Sivaramakrishnan, J. V. Michael, A. F. Wagner, R. Dawes, A. W. Jasper, L. B. Harding, Y. Georgievskii, and S. J. Klippenstein, Combust. Flame **158**, 618 (2011).
[18] S. D. Tommaso, P. Rotureau, O. Crescenzic, and C. Adamo, Phys. Chem. Chem. Phys. **13**, 14636 (2011).
[19] S. A. Carr, T. J. Still, M. A. Blitz, A. J. Eskola, M. J. Pilling, P. W. Seakins, R. J. Shannon, B. Wang, and S. H. Robertson, J. Phys. Chem. A **117**, 11142 (2013).
[20] S. Di Tommaso, P. Rotureau, W. Benaissa, P. Gruez, and C. Adamo, Energy Fuels **28**, 2821 (2014).
[21] W. K. Metcalfe, S. M. Burke, S. S. Ahmed, and H. J. Curran, Int. J. Chem. Kinet. **45**, 638 (2013).
[22] S. L. Fischer, F. L. Dryer, and H. J. Curran, Int. J. Chem. Kinet. **32**, 713 (2000).
[23] Z. Zhao, M. Chaos, A. Kazakov, and F. L. Dryer, Int. J. Chem. Kinet. **40**, 1 (2008).
[24] A. S. Tomlin, E. Agbro, V. Nevrly, J. Dlabka, and M. VaŠinek, Int. J. Chem. Kinet. **46**, 662 (2014).
[25] X. L. Zheng, T. F. Lu, C. K. Law, C. K. Westbrook, and H. J. Curran, Proc. Combust. Inst. **30**, 1101 (2005).
[26] D. Liu, J. Santner, C. Togbé, D. Felsmann, J. Koppmann, A. Lackner, X. Yang, X. Shen, Y. Ju, and K. Kohse-Höinghaus, Combust. Flame **160**, 2654 (2013).
[27] O. Welz, J. D. Savee, D. L. Osborn, S. S. Vasu, C. J. Percival, D. E. Shallcross, and C. A. Taatjes, Science **335**, 204 (2012).
[28] C. A. Taatjes, O. Welz, A. J. Eskola, J. D. Savee, D. L. Osborn, E. P. F. Lee, J. M. Dyke, D. W. K. Mok, D. E. Shallcross, and C. J. Percival, Phys. Chem. Chem. Phys. **14**, 10391 (2012).
[29] A. Jalan, I. M. Alecu, R. Meana-Pañeda, J. Aguilera-Iparraguirre, K. R. Yang, S. S. Merchant, D. G. Truhlar, and W. H. Green, J. Am. Chem. Soc. **135**, 11100 (2013).
[30] A. W. Jasper, S. J. Klippenstein, L. B. Harding, and B. Ruscic, J. Phys. Chem. A 111, 3932 (2007).
[31] L. B. Harding, S. J. Klippenstein, and A. W. Jasper, Phys. Chem. Chem. Phys. **9**, 4055 (2007).
[32] J. M. L. Martin and O. Uzan, Chem. Phys. Lett. **282**, 16 (1998).
[33] C. F. Goldsmith, G. R. Magoon, and W. H. Green, J. Phys. Chem. A **116**, 9033 (2012).
[34] F. L. Hirshfeld, Theor. Chim. Acta **44**, 129 (1977).
[35] Z. Wang, L. Zhang, and F. Zhang, J. Phys. Chem. A **118**, 6741 (2014).
[36] C. Fonseca Guerra, J. W. Handgraaf, E. J. Baerends, and F. M. Bickelhaupt, J. Comput. Chem. **25**, 189 (2004).
[37] M. J. Frisch, G. W. Trucks, H. B. Schlegel, G. E.Scuseria, M. A. Robb, J. R. Cheeseman, G. Scalmani, V. Barone, B. Mennucci, G. A. Petersson, H. Nakatsuji, M. Caricato, X. Li, H. P. Hratchian, A. F. Izmaylov, J. Bloino, G. Zheng, J. L. Sonnenberg, M. Hada, M. Ehara, K. Toyota, R. Fukuda, J. Hasegawa, M. Ishida, T. Nakajima, Y. Honda, O. Kitao, H. Nakai, T. Vreven, J. A. Jr. Montgomery, J. E. Peralta, F. Ogliaro, M. Bearpark, J. J. Heyd, E. Brothers, K. N. Kudin, V. N. Staroverov, R. Kobayashi, J. Normand, K. Raghavachari, A. Rendell, J. C. Burant, S. S. Iyengar, J. Tomasi, M. Cossi, N. Rega, J. M. Millam, M. Klene, J. E. Knox, J. B. Cross, V. Bakken, C. Adamo, J. Jaramillo, R. Gomperts, R. E. Stratmann, O. Yazyev, A. J. Austin, R. Cammi, C. Pomelli, J. W. Ochterski, R. L. Martin, K. Morokuma, V. G. Zakrzewski, G. A. Voth, P. Salvador, J. J. Dannenberg, S. Dapprich, A. D. Daniels, Ö. Farkas, J. B. Foresman, J. V. Ortiz, J. Cioslowski, and D. J. Fox, *Gaussian 09, Revision B.01*, Wallingford, CT: Gaussian Inc., (2009).
[38] H. J. Werner, P. J. Knowles, G. Knizia, F. R. Manby, and M. Schutz, *MOLPRO, version 2010.1*, www.molpro.net.
[39] C. Eckart, Phys. Rev. **35**, 1303 (1930).
[40] R. H. Wentorf, R. J. Buehler, J. O. Hirschfelder, and C. F. Curtiss, J. Chem. Phys. **18**, 1484 (1950).
[41] J. R. Welty, C. E. Wicks, R. E. Wilson, and G. L. Rorrer, *Fundamentals of Momentum Heat and Mass Transfer*, New York: John Wiley & Sons Ltd., (2001).
[42] L. Constantinou and R. Gani, AICHE J. **40**, 1697 (1994).
[43] Y. Georgievskii, J. A. Miller, M. P. Burke, and S. J. Klippenstein, J. Phys. Chem. A **117**, 12146 (2013).
[44] P. J. Linstrom and W. G. Mallard, http://webbook.nist.gov/chemistry/, (2005).
[45] H. Hou, J. Li, X. Song, and B. Wang, J. Phys. Chem. A **109**, 11206 (2005).
[46] J. Matthews, A. Sinha, and J. S. Francisco, J. Chem. Phys. **122**, (2005).
[47] D. Chen, H. Jin, Z. Wang, L. Zhang, and F. Qi, J. Phys. Chem. A **115**, 602 (2011).

DOI:10.1063/1674-0068/28/cjcp1503053